

# Sorbitol-Based Glass Matrices Enable Dynamic Nuclear Polarization beyond 200 K

Faith J. Scott, Samuel Eddy, Terry Gullion,\* and Frédéric Mentink-Vigier\*

Cite This: *J. Phys. Chem. Lett.* 2024, 15, 8743–8751

Read Online

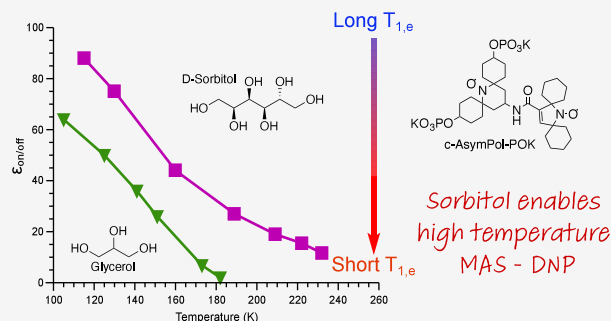
ACCESS |

Metrics & More

Article Recommendations

Supporting Information

**ABSTRACT:** In magic angle spinning dynamic nuclear polarization (MAS-DNP) experiments, paramagnetic species are often dispersed in rigid glass-forming matrices such as glycerol/water mixtures, but their modest glass-transition temperature ( $T_g$ ) restricts the viable temperature range for MAS-DNP. To expand applications of DNP at higher temperatures, new matrices and physical insights are required. Here we demonstrate that sorbitol,  $T_g \approx 267$  K, advantageously replaces glycerol,  $T_g \approx 190$  K, to carry out DNP at higher temperature while maintaining an identical  $^{13}\text{C}$  NMR spectrum footprint and thus minimizing spectral overlap. DNP stops being effective in glycerol/water at  $\sim 180$  K, but sorbitol/DMSO gives a significant enhancement at 230 K with AsymPol-POK biradicals at 600 MHz/395 GHz. For the first time, a simple analytical model is proposed that provides physical insights and explains the effect of biradical concentration, the temperature dependence of the enhancement, the signal buildup times, and the enhanced signal-to-noise ratio. The model reveals that electron spin relaxation is the limiting factor for high-temperature DNP in the case of AsymPol-POK. We showcase the efficacy of this new DNP formulation on an intriguing chitin sample extracted from cicada exoskeleton which allowed for the recording of rapid heteronuclear correlation spectra at 100 and 225 K.



Solid-state nuclear magnetic resonance (NMR) has witnessed a breakthrough with the development of magic angle spinning dynamic nuclear polarization (MAS-DNP). DNP transfers the polarization from unpaired electron spins to the surrounding nuclear spins, leading to unprecedented NMR sensitivity.<sup>1–6</sup> In modern MAS-DNP, unpaired electron spins are provided by biradicals added as dopants to the targeted samples.<sup>7–10</sup> These biradicals are dispersed in a frozen, glass-forming matrix that must be compatible with the target sample, and DNP is carried out at 100 K on commercial systems.<sup>11,12</sup> For optimal MAS-DNP, this glass-forming matrix must (i) dissolve the biradical during its formation, (ii) preserve the sample,<sup>13</sup> (iii) have a high-enough glass-transition temperature,  $T_g > 130$  K, to favor long electron spin relaxation,<sup>14</sup> (iv) be transparent to the irradiation frequency used to drive the electron spin transition,<sup>15</sup> and (v) have limited NMR spectral overlap with the signal of the targeted sample. Due to these constraints, there are limited possibilities for systems that are hydrophilic. While matrices composed of glycerol/water or dimethyl sulfoxide (DMSO)/water are the go-to solutions for MAS-DNP, their relatively low  $T_g < 170$  K<sup>16</sup> limits the temperature range where MAS-DNP can be applied. MAS-DNP experiments are often carried out at  $\sim 100$  K, requiring high liquid nitrogen consumption,<sup>12,17–19</sup> slow sample spinning speed,<sup>11,19,20</sup> and induced phase transitions/mobility changes<sup>21–23</sup> and/or limiting the spectral resolution for mobile samples.<sup>21,22,24</sup> The impact is particularly severe for some

biological samples, and it has been demonstrated that higher temperature improves the resolution of biological samples.<sup>21,24–27</sup> For these reasons, glass matrices and biradicals able to generate a sizable MAS-DNP enhancement at higher temperature should be actively studied.

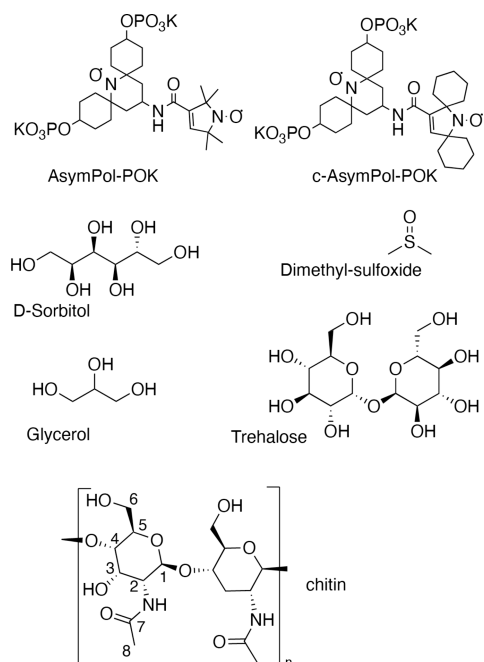
We recently observed that  $\alpha$ -chitin samples appear to be undergoing dynamical changes in the temperature range from 180 to 230 K (vide infra), which triggered this work focused on higher-temperature DNP. Potential matrices with higher glass-transition temperatures, such as trehalose, orthoterphenyl (OTP), polystyrene, and sucrose octo-acetate, have been reported in the EPR literature.<sup>14,28–31</sup> They all have glass-transition temperatures of  $T_g > 200$  K,<sup>14,32</sup> and thus some have been used for DNP at temperature  $>200$  K. OTP was first shown to enable DNP up to room temperature for material science applications,<sup>32,33</sup> while trehalose enables DNP at 230 K for biological applications.<sup>34</sup> Unfortunately, these aforementioned matrices result in  $^{13}\text{C}$  NMR signals that often overlap with signals from the target sample (so-called spectral

Received: July 12, 2024  
Revised: August 12, 2024  
Accepted: August 14, 2024  
Published: August 20, 2024



crowding). For example trehalose and chitin overlap completely, making the analysis challenging or else requiring special pulse sequences or labeling to eliminate the unwanted signals.<sup>35–37</sup> In contrast, glycerol and DMSO have simple NMR spectra that do not overlap significantly with other biological samples, including carbohydrates,<sup>38</sup> and have therefore been the go-to solution for hydrophilic samples.<sup>6,39,40</sup> D-Sorbitol (hereafter referred to as sorbitol) minimizes spectral overlap while providing a relatively high  $T_g$  of 267 K<sup>41</sup> as compared to that of glycerol ( $T_g = 190$  K).<sup>42</sup> Sorbitol is a linear polyol, like glycerol (Scheme 1), and it presents in the solid

**Scheme 1. Chemical Structure of the Biradical and Solvent/Glassing Agents Used for MAS-DNP and (1 → 4)-Chitin**



state only two  $^{13}\text{C}$  NMR signals located at the same positions as those of glycerol ( $\sim 70$  and  $62$  ppm). The strong hydrogen-bond network in the sorbitol enables a stiff glass and longer electron relaxation times.<sup>14,30,31</sup> To the best of our knowledge and despite its simplicity, sorbitol has never been used as a glassing agent for MAS-DNP until now.

In this Letter, we describe different formulations using sorbitol for MAS-DNP. We also provide a rational analysis of the DNP mechanism and sensitivity as a function of the temperature. Sorbitol, combined with water or DMSO, can be used as an efficient DNP matrix to carry out experiments at up to  $\sim 230$  K and with a magnetic field of  $14.1$  T/ $395$  GHz if it is used with a polarizing agent that hyperpolarizes the nuclei quickly such as the AsymPol family.<sup>43,44</sup> We developed a novel rate equation model to predict and analyze the DNP performance of the formulation as a function of temperature. The model, developed for AsymPols,<sup>45</sup> provides new physical insights into the temperature dependence of the enhancement and the build-up times and quantitatively predicts the evolution of the experimental signal-to-noise ratio. The model reveals the role of biradical concentration and the electron relaxation time in those fast-hyperpolarizing biradicals, giving a pathway to improve the DNP at a higher temperature. The merit of this sample formulation is demonstrated on chitin extracted from cicada exoskeleton where variable-temperature

MAS-DNP enables us to observe dynamical changes as a function of temperature via  $^1\text{H}$ – $^{13}\text{C}$  experiments. We report for the first time high-resolution  $^{13}\text{C}$ – $^1\text{H}$  heteronuclear correlation spectroscopy (HETCOR) on a biological sample at  $\sim 225$  K under DNP conditions.

**Results.** Sorbitol is a polyol with a high melting temperature of  $\sim 368$  K ( $95$  °C) (see Scheme 1). Upon melting, it forms a viscous solution that must be quickly cooled to form a glass. Reducing the melting temperature and viscosity is required to ease sample preparation. When sorbitol is mixed with a solvent, the melting temperature decreases and a glass can be formed under slow cooling conditions. An obvious solvent to achieve this is water; however, the introduction of water can decrease the  $T_g$  significantly,<sup>46</sup> and good glass formulation may be obtained only under a controlled atmosphere, as demonstrated for trehalose (Scheme 1).<sup>34</sup> Sorbitol/glycerol can form a good glass<sup>41</sup> but is not practical to use due to its high viscosity. To ease the sample preparation, we settled on a simple formulation of sorbitol/DMSO. This matrix has a more fluid formulation for easier sample packing and enables our analysis of the DNP mechanism as a function of the temperature.

To observe the changes in the chitin's dynamics and structure between  $100$  and  $230$  K, we first determined the appropriate sorbitol/DMSO ratio mixture. To estimate the  $T_g$  of a sorbitol/DMSO mixture, we tested the validity of the Gordon–Taylor equation<sup>47</sup> combined with the Simha–Boyer rule.<sup>48,49</sup> The resulting equation predicts the approximate  $T_g$  for a polymer mixture<sup>50</sup> but can be applied to some molecular binary mixtures<sup>51</sup>

$$T_g = \frac{wT_{g,1} + k(1-w)T_{g,2}}{w + k(1-w)}, \quad k = \frac{T_{g,1}\rho_1}{T_{g,2}\rho_2} \quad (1)$$

where  $w$  is the mass fraction of compound 1 and  $T_{g,i}$  and  $\rho_i$  are the glass transition and density of compound  $i$ . The calculated glass-transition temperatures for several relevant mixtures are shown in Figure S1. Equation 1 reproduces semiquantitatively the experimental results of the sorbitol/glycerol mixture<sup>41</sup> and trehalose/water<sup>52</sup> and predicts the glass-transition temperature of glycerol/deuterated water, with  $T_g \approx 163$  K for a glycerol/ $\text{D}_2\text{O}$  mixture (6/4 vol % or a glycerol mass fraction of  $0.65$ ,  $T_{g,\text{gly}} = 190$  K).<sup>16,41,53</sup> Equation 1 predicts  $T_g \approx 210$  K for sorbitol/ $\text{H}_2\text{O}$  (8:2 mass %), assuming  $T_{g,\text{H}_2\text{O}} \approx 135$  K,<sup>42</sup> close to the experimental value of  $\sim 210 \pm 4$  K for (8:2 mass %).<sup>54</sup> A mass ratio of sorbitol/DMSO (8:2 mass %) would instead lead to a glass-transition temperature of about  $225$  K (assuming  $T_{g,\text{DMSO}} \approx 150$  K).<sup>42</sup> To avoid the fast relaxation that protonated DMSO methyl groups can generate, we replaced DMSO with DMSO- $\text{D}_6$ , and the corresponding proton concentration is  $[\text{H}] = 50$  M. In addition, to overcome the limitation induced by high proton concentration,<sup>45,55</sup> we used the biradicals AsymPol-POK (ASP) and c-AsymPol-POK (c-ASP)<sup>56</sup> (see Scheme 1) which showed limited sensitivity to the sample's proton concentration.<sup>56,57</sup> Both biradicals can be used in fully protonated media without leading to a significant loss of hyperpolarization capabilities, especially under a high magnetic field, here  $14.1$  T.<sup>56</sup> In addition, these biradicals can hyperpolarize the medium very quickly<sup>45</sup> and thus are less sensitive to the intrinsic relaxation times of the samples<sup>58</sup> (*vide infra*).

The MAS-DNP performance as a function of temperature was then carried out for two different c-AsymPol-POK concentrations and for the two matrices, sorbitol/DMSO- $\text{D}_6$

**Table 1. Enhancement ( $\epsilon_{\text{on/off}}$  and Buildup Time ( $T_B$ ) for Different Biradicals and Matrix Compositions**

Sample	$\epsilon_{\text{on/off}}$ $T_B$ (s) at $\sim 110$ K	$\epsilon_{\text{on/off}}$ $T_B$ (s) at 230 K
5 mM c-AsymPol-POK in sorbitol/DMSO-D <sub>6</sub> (8:2)	88, 4.3 (113 K)	11.6, 2.8
10 mM c-AsymPol-POK in sorbitol/DMSO-D <sub>6</sub> (8:2)	80, 1.6 (113 K)	19, 1.4
5 mM c-AsymPol-POK in sorbitol/D <sub>2</sub> O (8:2)	66, 3.5 (105 K)	4.7, 1.1
10 mM AsymPol-POK in glycerol-D <sub>8</sub> /D <sub>2</sub> O/H <sub>2</sub> O (6:3:1 vol %)	67, 1.8 ( $\sim 105$ K)	-

( $[^1\text{H}] = 50$  M) and sorbitol/D<sub>2</sub>O ( $[^1\text{H}] = 48$  M). The sample temperature was monitored by using KBr crystals coated with a thin layer of clear nail polish at the bottom of the rotor. In a fully packed rotor, the optimal  $\mu\text{w}$  irradiation power was low (7–9 W), leading to suboptimal enhancements (*ca.* 50). This correlated with a significant sample temperature increase ( $\sim 20$  K, see SI), and we attributed this to the  $\mu\text{w}$  absorption of polyols in the DNP range.<sup>59</sup> Using our previously published method,<sup>60</sup> the dielectric constant at  $\sim 395$  GHz of a mixture of sorbitol/water (1:1) was found to be  $n = 1.98$  with  $k = 10^{-2}$ . We also observed in the case of the 10 mM AsymPol-POK in glycerol-D<sub>8</sub>/D<sub>2</sub>O/H<sub>2</sub>O (6:3:1 vol %) that the enhancements were reduced when adding coated KBr crystals from 80 to 67. To minimize the sample absorption, we added crushed sapphire crystal to the rotor ( $\sim 1/3$  of the sample volume),<sup>61</sup> which enabled using high  $\mu\text{w}$  irradiation power ( $\sim 15$  W) and more reproducible enhancement results.

The enhancement and buildup times at  $\sim 110$  and 230 K for three samples are reported in Table 1. At  $\sim 110$  K, all matrix compositions offer good enhancement,  $\sim 70$ – $90$ , similar to glycerol/water mixtures.<sup>56</sup> At 110 K, the biradical concentration does not appear to influence the enhancement substantially; however, it does at 230 K: for 5 mM biradical concentration, the enhancement is lower in sorbitol/D<sub>2</sub>O as compared to the sorbitol/DMSO-D<sub>6</sub> with enhancements of  $\sim 5$  and 11, respectively. At 230 K, the enhancement is higher for 10 mM and reaches  $\sim 19$ . These enhancements compare favorably with state-of-the-art methods using trehalose,<sup>34</sup> albeit at higher magnetic field (14.1 T, vs 9.4 T) and using larger rotors (3.2 vs 1.3 mm). For comparison, a 10 mM AsymPol-POK solution in a glycerol/D<sub>2</sub>O (6:4 vol %) matrix is completely inefficient above 180 K (see SI, Figure S2), which agrees with previous work.<sup>21,62</sup>

The buildup times are longer for the sample with a biradical concentration of 5 mM than for the sample with a 10 mM concentration in the sorbitol/DMSO-D<sub>6</sub> matrix. This is observed at both  $\sim 110$  and 230 K and is consistent with previous observations in glycerol/water mixtures.<sup>57</sup> At 100 K, the buildup time for the 5 mM sample in the sorbitol/D<sub>2</sub>O matrix is shorter than that for sorbitol/DMSO-D<sub>6</sub>, and it is even shorter than that for the 10 mM sorbitol/DMSO-D<sub>6</sub> sample at 230 K.

To complete the picture, the temperature dependences of the enhancement and buildup time are reported in Figure 1. The normalized enhancement for the 5 mM samples has a more severe temperature dependence as compared to that of the 10 mM sample (Figure 1 (a)). The temperature dependence of the 10 mM sample shows similarity with the dependence observed for trehalose,<sup>34</sup> indicating similarities in the underlying physical process.

The steeper temperature dependence of the enhancement for the sample with a 5 mM biradical concentration versus the one that is 10 mM in sorbitol/DMSO-D<sub>6</sub> indicates that a biradical concentration of 5 mM is not as efficient to hyperpolarize at higher temperature. This could be attributed

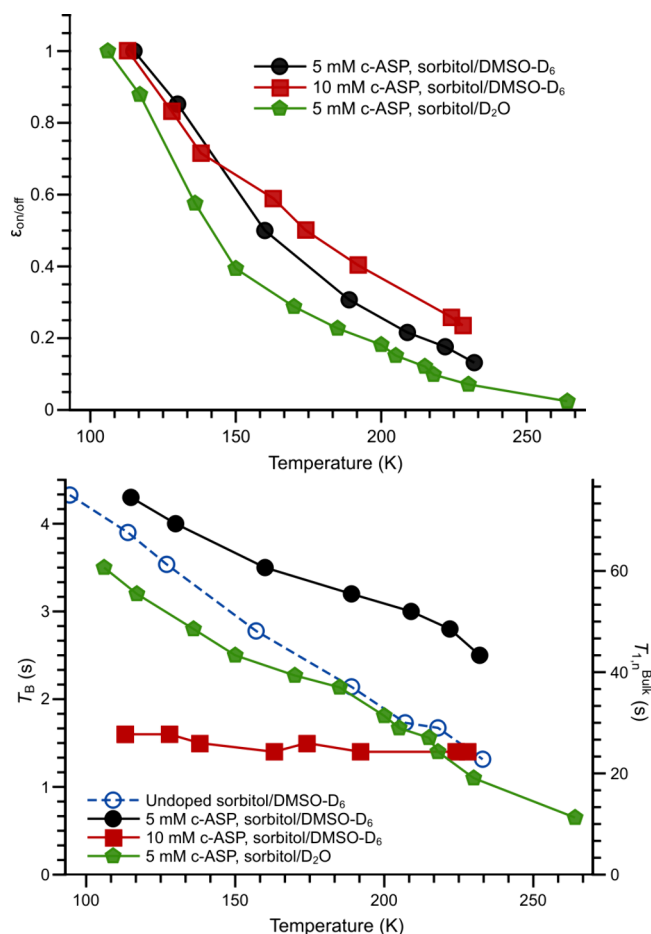


**Figure 1.** Evolution of the enhancement (top) and buildup time (bottom) as a function of the sample's temperature. Black circles, 5 mM c-AsymPol-POK (c-ASP) in sorbitol/DMSO-D<sub>6</sub>; red squares, 10 mM c-AsymPol-POK in sorbitol/DMSO-D<sub>6</sub>; and green hexagons, 5 mM c-AsymPol-POK in sorbitol/D<sub>2</sub>O. The buildup time of undoped sorbitol/DMSO-D<sub>6</sub> is indicated by the open blue circles.

to faster proton relaxation that is not compensated for by the CE mechanism. To confirm this hypothesis, the proton relaxation time of an undoped sorbitol/DMSO-D<sub>6</sub> and the build-up times of doped samples were measured as a function of temperature for all samples (see Figure 1 (b)). The nuclear relaxation time in the undoped sample decreased from 75 to 25 s between 100 and 230 K. In parallel, the build-up time of the sample with 5 mM follows the same trend and decreases from 4.5 to 2.7 s, while the build-up time in the sample with 10 mM biradical is unchanged.

The build-up time behavior can be semiquantitatively simulated using an analytical rate equation model that assumes that the biradical transfers its polarization difference to the protons on the biradical and to surrounding protons via the cross-effect.<sup>45</sup> In the case of AsymPol, we showed that the cross-effect mechanism involves a direct flow of polarization

from the electron spins to the surrounding nuclei, and the equations can then be simplified as (see the SI)

$$\frac{dP_n^{\text{solv}}}{dt} = -xR_{\text{CE}}^{\text{solv}}(P_n^{\text{solv}} - \Delta P_e) - R_{1,n}^{\text{solv}}(P_n^{\text{solv}} - P_{n,B}) \quad (2)$$

where  $\Delta P_e$  is the electron spin polarization difference<sup>63–65</sup> that is transferred to the fraction,  $x$ , of solvent nuclear spins surrounding the biradicals at a rate  $R_{\text{CE}}^{\text{solv}}$ . The nuclear spins undergo relaxation at a rate  $R_{1,n}^{\text{solv}}$  and attempt to return to the thermal equilibrium value,  $P_{n,B}$ . Among the assumptions, spin diffusion is supposed to be fast compared to nuclear relaxation. The solution to this equation is simply

$$P_n^{\text{solv}}(t) = \frac{xR_{\text{CE}}^{\text{solv}}\Delta P_e + R_{1,n}^{\text{solv}}P_{n,B}}{xR_{\text{CE}}^{\text{solv}} + R_{1,n}^{\text{solv}}}(1 - e^{-(xR_{\text{CE}}^{\text{solv}} + R_{1,n}^{\text{solv}})t}) \quad (3)$$

Using the determined cross-effect rate  $R_{\text{CE}}^{\text{solv}} \approx 15.8 \text{ s}^{-1}$ ,<sup>45</sup> the fraction of solvent proton spins undergoing the cross-effect is  $x = 1.6\%$  for 5 mM, or 3.2% for 10 mM, and for the measured relaxation time of the solvent  $1/T_{1,n}^{\text{Bulk}} = R_{1,n}^{\text{solv}}$ , the model predicts a buildup time of  $T_B = 3.62 \text{ s}$  at 113 K and  $T_B = 3.15 \text{ s}$  at 230 K for the 5 mM sample. For 10 mM, it predicts  $T_B = 1.8 \text{ s}$  and  $T_B = 1.66 \text{ s}$  at 113 and 230 K, respectively. These predicted values align remarkably well with the experiments considering the numerous simplifications the model uses (details in the SI). This indicates that the model captures most of the underlying spin dynamics. Equation 3 confirms that for the 5 mM sample the faster nuclear relaxation time is in part responsible for the faster buildup times. The enhancements at  $\sim 113 \text{ K}$  can be reproduced with  $\Delta P_e(113 \text{ K})/P_{n,B} = 85$  to yield enhancements of  $\sim 81$  and 83 for 5 and 10 mM, respectively, using eq 3. This model can be used to assess the impact of the nuclear spin relaxation on the enhancements as a function of temperature. If we assume that  $\Delta P_e/P_{n,B}$  is constant at all temperatures by neglecting the changes in electron relaxation times, then the predicted enhancements at 230 K are

$$\frac{xR_{\text{CE}}^{\text{solv}}\Delta P_e(113 \text{ K})/P_{n,B} + R_{1,n}^{\text{solv}}(230 \text{ K})}{xR_{\text{CE}}^{\text{solv}} + R_{1,n}^{\text{solv}}(230 \text{ K})} \approx 71(5 \text{ mM}) \text{ and } 76(10 \text{ mM}) \quad (4)$$

These values are much higher than the experimental values, which means that  $\Delta P_e/P_{n,B}$  is not constant and the shortening of the nuclear relaxation times is not the only source of enhancement reduction.

$\Delta P_e/P_{n,B}$ , the driver of the cross-effect mechanism, is the result of a complex balance among the  $\mu w$  rotor events, the dipolar/exchange rotor events, and the electron relaxation times  $T_{1,e}$ .<sup>63,66</sup> As shown in the Supporting Information, when the dipolar/exchange rotor events are adiabatic, as it is mostly the case with the AsymPols, it is possible to determine the temperature dependence of  $\Delta P_e$ . Based on the estimations by Thurber/Tycko<sup>65</sup> of the average number of  $\mu w$  rotor events of  $\sim 2$  per crystal orientation, one can obtain

$$\frac{\Delta P_e}{P_{n,B}} = \frac{\omega_e}{\omega_I} \left( 1 - \frac{\left( 1 - \exp\left(-\frac{\tau_r}{2T_{1,e}}\right) \right)}{\left( 1 - (1 - 2\epsilon_{\mu w}(\tau_r)) \exp\left(-\frac{\tau_r}{2T_{1,e}}\right) \right)} \right) \quad (5)$$

where  $\tau_r$  is the rotor period,  $\epsilon_{\mu w}$  is the Landau–Zener adiabaticity probability<sup>58,63,65</sup> and is a function of  $\tau_r$  and  $\omega_e/1$

represents the Larmor frequencies of the electron and nuclear spins. The temperature dependence of  $T_{1,e}$  obtained via the work of Eaton and Eaton on the temperature dependence of nitroxide electron spin relaxation in the glassy state is dominated by the Raman process<sup>14,28,30</sup>

$$\frac{T_{1,e}(T_a)}{T_{1,e}(T_b)} = \left( \frac{T_a}{T_b} \right)^n \quad (6)$$

where  $n = -2$ , which gives the relative evolution of the electron spin relaxation time in a glassy state as a function of temperature.<sup>14,62</sup> Equations 5 and 6 allows us to determine  $T_{1,e}(230 \text{ K}) \approx 0.2T_{1,e}(113 \text{ K})$ , which yields  $\Delta P_e/P_{n,B}(230 \text{ K}) \approx 0.1\Delta P_e/P_{n,B}(113 \text{ K})$  for 8 kHz and  $T_{1,e} = 0.3 \text{ ms}$  (see the SI). Using these values, the predicted enhancements are

$$\frac{R_{\text{CE}}^{\text{solv}}x\Delta P_e(230 \text{ K})/P_{n,B} + R_{1,n}^{\text{solv}}(230 \text{ K})}{xR_{\text{CE}}^{\text{solv}} + R_{1,n}^{\text{solv}}(230 \text{ K})} \approx 14(5 \text{ mM}) \text{ and } 16(10 \text{ mM}) \quad (7)$$

in better agreement with the experimental values of  $\sim 12$  and 19.

Despite its simplicity, the model compares favorably with the experiment (see Figure S4). It should be made clear, however, that the enhancements predicted by eq 3 ignore the effect of depolarization. Fortunately, AsymPols does not depolarize significantly, which allows us to neglect this factor.<sup>43,56</sup> All in all, the model shows that the main reason for the decay of the enhancement arises from the reduction of  $\Delta P_e/P_{n,B}$ , and a minor contribution comes from the changes in the nuclear relaxation times, which has more impact on the 5 mM samples than the 10 mM sample.

The viability of MAS-DNP at a higher temperature generally relies on the signal-to-noise ratio (SNR) of the experiment. Here, the evolution of the SNR as a function of temperature is shown in Figure 2 for the 10 mM sample. The normalized SNR without  $\mu w$ ,  $\text{SNR}_{\text{off}}(T)$ , has a weak temperature dependence, while the SNR under  $\mu w$  irradiation,  $\text{SNR}_{\text{on}}$

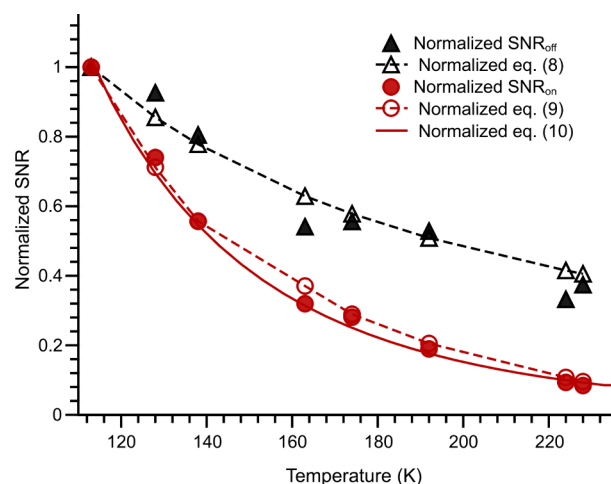


**Figure 2.** Evolution of the signal-to-noise ratio (SNR) as a function of temperature for 10 mM c-AsymPol-POK in sorbitol/DMSO- $D_6$ . Solid black triangles correspond to  $\mu w$  off, and red circles, to  $\mu w$  on. Dotted lines correspond to eq 8 (open black triangles with dashed lines), eq 9 (red open circles with dashed lines), and eq 10 (closed red circles and solid line). For normalization, the reference temperature was  $T_{\text{ref}} = 113 \text{ K}$ .

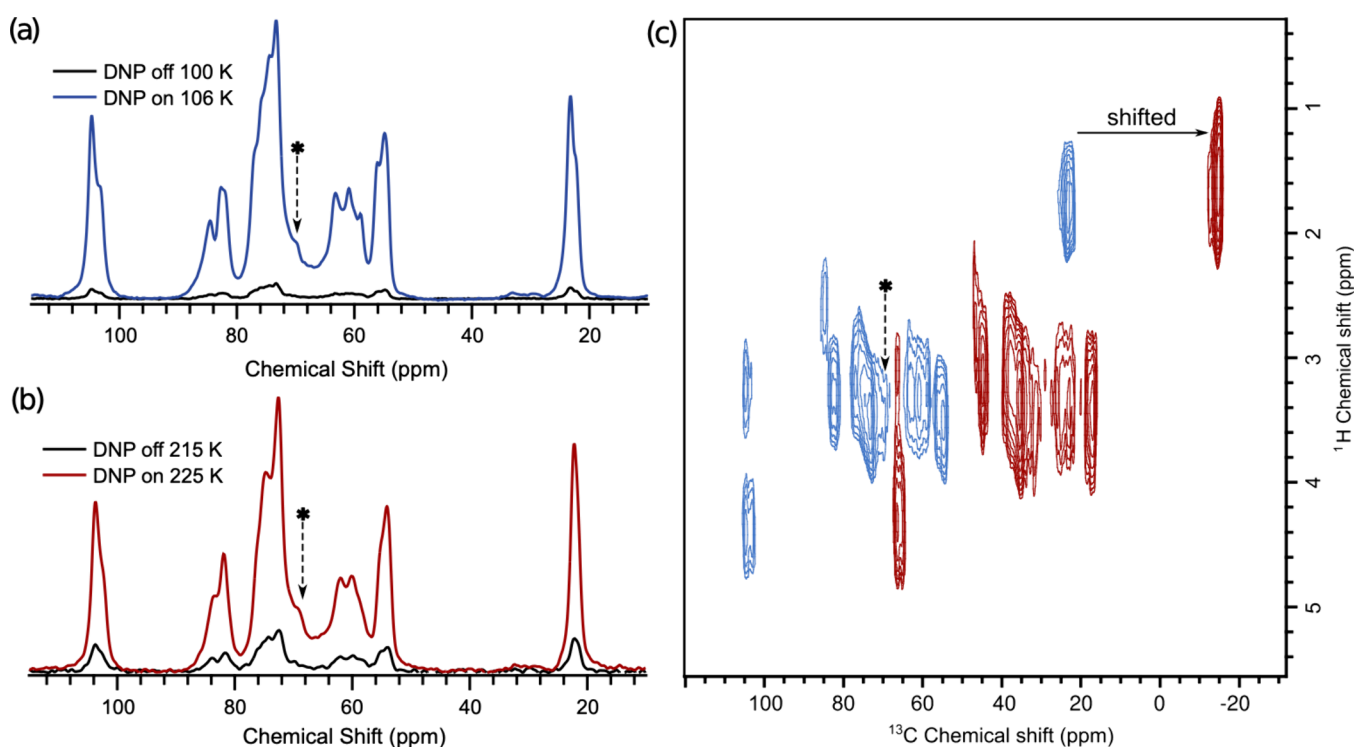


**Figure 3.** (a)  $^{13}\text{C}$  CP NMR spectra of the cicada chitin at  $\sim 106$  K (blue is  $\mu\text{w}$  on at  $\sim 100$  K; black is  $\mu\text{w}$  off). (b) Same at  $\sim 225$  K (red is  $\mu\text{w}$  on at  $\sim 215$  K; black is  $\mu\text{w}$  off). (c) DNP enhanced heteronuclear correlation of chitin at 106 K (blue) and 225 K (red). The 225 K spectrum is shifted to the right for the sake of clarity. The asterisk represents one of the sorbitol signals.

( $T$ ), decreases more rapidly. The SNR temperature dependence can be quantitatively predicted. The NMR signal intensity,  $S$ , is proportional to the product of the nuclear spin polarization dependence with temperature,  $P_{\text{n,off}}(T) \propto 1/T$ , and the square root of the quality factor,  $Q$ , of the radio frequency circuit of the probe  $\sqrt{Q}$ :  $S(T) \propto \frac{\sqrt{Q(T)}}{T}$ . Note that the variation of  $\sqrt{Q}$  over 100 to 230 K ( $\sim 20\%$ ) is modest and thus negligible. The noise in the radio frequency circuit is given by  $\text{noise}(T) \propto \sqrt{kT + NF_p}$ , where  $NF_p$  is the preamplifier noise figure, which has an equivalent temperature of  $T_p \approx 120$  K (for  $\sim 1.5$  dB). This leads to

$$\text{SNR}_{\text{off}}(T) \propto \frac{1}{T(T + T_p)^{0.5}} \quad (8)$$

The  $\mu\text{w}$  on  $\text{SNR}_{\text{on}}(T)$  can be simply deduced as

$$\text{SNR}_{\text{on}}(T) \propto \frac{\epsilon_{\text{on/off}}}{T(T + T_p)^{0.5}} \quad (9)$$

Using eqs 4 and 5, the relative  $\text{SNR}_{\text{on}}$  for the 10 mM sample is given by

$$\frac{\text{SNR}_{\text{on}}(T)}{\text{SNR}_{\text{on}}(T_{\text{ref}})} = \frac{T_{\text{ref}} \Delta P_c(T)}{T \Delta P_c(T_{\text{ref}})} \left( \frac{T_{\text{ref}} + T_p}{T + T_p} \right)^{0.5} \quad (10)$$

The corresponding normalized curves are reported in Figure 2. The temperature  $T_{\text{ref}} = 113$  K was chosen as a reference point for normalization. Equations 8, 9, and 10 have very good agreement with the experiments. Equation 10, combined with eqs 5 and 6, can predict for the first time the behavior of the experimental  $\text{SNR}_{\text{on}}$  and the sensitivity of the MAS-DNP experiment.

To verify the viability of high-temperature MAS-DNP, DMSO- $\text{D}_6$ /sorbitol combined with AsymPol was subsequently used to enhance the spectra of a biomaterial,  $\alpha$ -chitin, extracted from the cicada exoskeleton. As changes in the spectra occur within the temperature range of 180–230 K, this requires the use of an appropriate glass matrix to carry out multidimensional experiments in natural abundance.  $^{13}\text{C}$  NMR signals of  $\alpha$ -chitin usually appear as single NMR resonances for the carbons forming the carbohydrate backbone.<sup>67–69</sup> However, at 100 K there are three resolved  $^{13}\text{C}$  resonances for the C4 ( $\sim 80$  ppm) and three resolved  $^{13}\text{C}$  resonances for the C6 ( $\sim 62$  ppm) carbon (see Scheme 1). This observation contradicts previous room-temperature reports. The sample's temperature may impact the dynamics, and at higher temperature, the signals become simpler. As shown in Figure 3 (a) and (b), the  $^{13}\text{C}$  CPMAS NMR spectra of chitin indeed change in the temperature range of 225 to 100 K. Unlike previously reported  $^{13}\text{C}$  NMR spectra, the 225 K spectrum shows two clearly resolved resonances for the carboxyl carbon and the C6 ( $\sim 62$  ppm) carbon instead of one resonance for each. This is observed in both neat and impregnated chitin (see SI, Figure S5). As the temperature is decreased, additional  $^{13}\text{C}$  resonances begin to appear for each of these carbon sites.

The chitin sample is challenging to hyperpolarize at 100 K. After optimization, a modest enhancement of  $\sim 19$  at 106 K (see Figure 3 (a)) was obtained with a buildup time of 1.6 s (fitted with a monoexponential) and an optimal 16 W of  $\mu\text{w}$  irradiation power at the probe base. The modest enhancement is explained by the fast  $^1\text{H}$  relaxation time in the pure chitin ( $T_{1,\text{H}}^{\text{chitin}}(100 \text{ K}) \approx 5$  s), which may be due to the methyl group dynamics. An enhancement is maintained at up to 225 K with a factor of 6 to 7 (see Figure 3 (b)) with a build-up time of 1.1 s (fitted with a monoexponential) and an optimal  $\mu\text{w}$  power of

12 W. The drop in enhancement from 113 to 225 K is consistent with the one observed for the 10 mM sample. Note that, as commonly observed for samples with  $\mu\text{m}$  scale thickness,<sup>70,71</sup> a biexponential fit is more appropriate to capture the slower component that represents  $\sim 30\%$  of the polarization buildup (see SI, Figure S6). The time savings obtained via DNP and accounting for the loss of sample volume with the sapphire particles amounts to factors of  $\sim 200$  and  $\sim 20$  at 100 and 230 K, respectively.

Figure 3 (c) shows  $^1\text{H}$ – $^{13}\text{C}$  HETCOR MAS-DNP for  $\alpha$ -chitin. At the optimal sensitivity, this enabled recording the HETCOR spectra at 106 and 225 K in under 28 and 72 min, respectively. The HETCOR reveals not only changes in the  $^{13}\text{C}$  spectra but also changes in the  $^1\text{H}$  spectra. Each  $^{13}\text{C}$  signal relates to a distinctive  $^1\text{H}$  resonance. To the best of our knowledge, these low-temperature  $^{13}\text{C}$  spectral features of chitin have not been observed before; a detailed analysis of the spectra will be the subject of a subsequent publication.

**Discussion.** All in all, sorbitol/DMSO or other sorbitol mixtures should be considered to be new tools to carry out MAS-DNP experiments at temperatures higher than 100 K. Through a new and simple model, we provide for the first time a quantitative analysis of the temperature dependence enhancement, the build-up time, and the SNR as a function of temperature. From these equations, we decoupled the impact on the enhancement of the biradical from the impact of the nuclear relaxation time. The signal-to-noise ratio analysis showed that raising the temperature will always yield lower SNR by up to a factor of  $>3$  when going from 100 to 300 K, and the reduction of the enhancement with increasing temperature is a challenge to overcome. As shown through the analytical model, the limiting factor for DNP at high temperature in our 10 mM samples is solely the fast electron relaxation times and not the combination of phase memory time and electron relaxation times<sup>33</sup> and/or nuclear relaxation times.<sup>62</sup> At a lower concentration, 5 mM, the nuclear relaxation times contribute to the reduction of the enhancement as well. Longer electron relaxation times and concentration  $\geq 10$  mM are key to unlocking the potential of higher-temperature DNP to favor both larger  $\Delta P_e(T)$  and  $\alpha$ . As such, the use of heterobiradicals<sup>72–75</sup> with longer relaxation times<sup>30</sup> and high solubility could yield higher enhancements only if the electron–electron couplings are strong as in the case of PyrroTriPol or TEMTriPols.<sup>72,73,75–77</sup> For material science applications, higher enhancement at 230 K was indeed obtained with HiTEK-2 at 18.8 T but using 95% deuterated OTP and a 1.3 mm rotor. Our work demonstrates that for a successful application in a protonated medium strong electron–electron coupling (or a lower magnetic field instrument)<sup>45</sup> will be required to favor large  $\alpha_{\text{CE}}^{\text{sol}}$ , and we anticipate that the high solubility of such a radical will be essential.<sup>73</sup> This also points out that small rotors are required to favor high-temperature DNP as better cooling and higher electron spin nutation can be obtained.<sup>60,78,78</sup>

To illustrate the viability of sample preparation with the sorbitol mixture, we applied it to one of nature's most abundant macromolecules. A sample of  $\alpha$ -chitin was used to illustrate the ability to carry out MAS-DNP experiments at up to  $\sim 225$  K on biological systems. We expect this matrix to have much broader interest, especially for biological applications. The ability to raise the temperature while maintaining high sensitivity may enable higher-resolution DNP on biological samples<sup>21,62</sup> if adequate sample preparation allows it. It can

also be used to analyze the dynamic properties of samples as a function of temperature under MAS-DNP conditions and extend the application of experiments such as SCREAM DNP.<sup>79–81</sup>

Finally, these matrices could enable efficient DNP with more moderate cooling requirements (in the range of 120–200 K), thereby cutting down on nitrogen consumption. In our experiments (not shown), this temperature can be reached with a single cold gas flow, as in conventional solid-state NMR instrumentation. This less stringent condition would enable higher spinning frequencies<sup>79–81</sup> that allow some recoupling pulse sequences, minimize spinning sidebands, and also provide better performance for the 0.7 and 1.3 mm DNP probes.<sup>82,83</sup> Finally, less nitrogen consumption would enable a lower running cost for MAS-DNP instruments, which may further the uptake of the technique, particularly outside of academia.

Sorbitol-based matrices have already illuminated the dynamic structure of chitin at 100 and 200 K, with minimal spectral overlap. Other systems can also benefit from this matrix, and it has the potential to lower DNP operational costs. Therefore, we believe that sorbitol-based matrices will be an important tool in the DNP technique toolbox.

## ■ ASSOCIATED CONTENT

### Supporting Information

The Supporting Information is available free of charge at <https://pubs.acs.org/doi/10.1021/acs.jpcllett.4c02054>.

Experimental details and derivation of the equations (PDF)

## ■ AUTHOR INFORMATION

### Corresponding Authors

Terry Gullion – Department of Chemistry, West Virginia University, Morgantown, West Virginia 26506, United States; [orcid.org/0000-0002-1899-6884](https://orcid.org/0000-0002-1899-6884); Email: [terry.gullion@mail.wvu.edu](mailto:terry.gullion@mail.wvu.edu)

Frédéric Mentink-Vigier – National High Magnetic Field Laboratory, Florida State University, Tallahassee, Florida 32310, United States; [orcid.org/0000-0002-3570-9787](https://orcid.org/0000-0002-3570-9787); Email: [fmentink@magnet.fsu.edu](mailto:fmentink@magnet.fsu.edu)

### Authors

Faith J. Scott – National High Magnetic Field Laboratory, Florida State University, Tallahassee, Florida 32310, United States; [orcid.org/0000-0003-3903-8842](https://orcid.org/0000-0003-3903-8842)

Samuel Eddy – Department of Chemistry, West Virginia University, Morgantown, West Virginia 26506, United States

Complete contact information is available at: <https://pubs.acs.org/10.1021/acs.jpcllett.4c02054>

### Notes

The authors declare no competing financial interest.

## ■ ACKNOWLEDGMENTS

The National High Magnetic Field Laboratory (NHMFL) is funded by the National Science Foundation Division of Materials Research (DMR-2128556) and the State of Florida. F.J.S. acknowledges support from a postdoctoral scholar award from the Provost's Office at Florida State University. A portion of this work was supported by NIH RM1-GM148766 and the European Union's Horizon 2020 Research and Innovation

Programme under grant agreement no. 101008500. F.M.-V. thanks Zhehong Gan for fruitful conversations and Daniel Lee for critical reading of the manuscript.

## REFERENCES

- (1) Ni, Q. Z.; Daviso, E.; Can, T. V.; Markhasin, E.; Jawla, S. K.; Swager, T. M.; Temkin, R. J.; Herzfeld, J.; Griffin, R. G. High Frequency Dynamic Nuclear Polarization. *Acc. Chem. Res.* **2013**, *46* (9), 1933–1941.
- (2) Rossini, A. J.; Zagdoun, A.; Lelli, M.; Lesage, A.; Copéret, C.; Emsley, L. Dynamic Nuclear Polarization Surface Enhanced NMR Spectroscopy. *Acc. Chem. Res.* **2013**, *46* (9), 1942–1951.
- (3) Lee, D.; Hediger, S.; De Paëpe, G. Is Solid-State NMR Enhanced by Dynamic Nuclear Polarization? *Solid State Nucl. Magn. Reson.* **2015**, *66–67*, 6–20.
- (4) Paioni, A. L.; Renault, M. A. M.; Baldus, M. DNP and Cellular Solid-State NMR. *eMagRes* **2018**, *7*, 51–62.
- (5) Rankin, A. G. M.; Trébosc, J.; Pourpoint, F.; Amoureux, J.-P.; Lafon, O. Recent Developments in MAS DNP-NMR of Materials. *Solid State Nucl. Magn. Reson.* **2019**, *101*, 116–143.
- (6) Chow, W. Y.; De Paëpe, G.; Hediger, S. Biomolecular and Biological Applications of Solid-State NMR with Dynamic Nuclear Polarization Enhancement. *Chem. Rev.* **2022**, *122* (10), 9795–9847.
- (7) Hu, K.-N.; Yu, H.; Swager, T. M.; Griffin, R. G. Dynamic Nuclear Polarization with Biradicals. *J. Am. Chem. Soc.* **2004**, *126* (35), 10844–10845.
- (8) Lilly Thankamony, A. S.; Wittmann, J. J.; Kaushik, M.; Corzilius, B. Dynamic Nuclear Polarization for Sensitivity Enhancement in Modern Solid-State NMR. *Prog. Nucl. Magn. Reson. Spectrosc.* **2017**, *102–103*, 120–195.
- (9) Casano, G.; Karoui, H.; Ouari, O. Polarizing Agents: Evolution and Outlook in Free Radical Development for DNP. *eMagRes* **2018**, *7*, 195–208.
- (10) Hediger, S.; Lee, D.; Mentink-Vigier, F.; De Paëpe, G. MAS-DNP Enhancements: Hyperpolarization, Depolarization, and Absolute Sensitivity. *eMagRes* **2018**, *7*, 105–116.
- (11) Rosay, M.; Tometich, L.; Pawsey, S.; Bader, R.; Schauwecker, R.; Blank, M.; Borchard, P. M.; Cauffman, S. R.; Felch, K. L.; Weber, R. T.; Temkin, R. J.; Griffin, R. G.; Maas, W. E. Solid-State Dynamic Nuclear Polarization at 263 GHz: Spectrometer Design and Experimental Results. *Phys. Chem. Chem. Phys.* **2010**, *12* (22), 5850.
- (12) Rosay, M.; Blank, M.; Engelke, F. Instrumentation for Solid-State Dynamic Nuclear Polarization with Magic Angle Spinning NMR. *J. Magn. Reson.* **2016**, *264*, 88–98.
- (13) Liao, S. Y.; Lee, M.; Wang, T.; Sergeyev, I. V.; Hong, M. Efficient DNP NMR of Membrane Proteins: Sample Preparation Protocols, Sensitivity, and Radical Location. *J. Biomol. NMR* **2016**, *64* (3), 223–237.
- (14) Eaton, S. S.; Eaton, G. R.; Harris, R. K.; Wasylishen, R. L. Relaxation Mechanisms. *eMagRes* **2016**, *5*, 1543–1556.
- (15) Nanni, E. A.; Barnes, A. B.; Matsuki, Y.; Woskov, P. P.; Corzilius, B.; Griffin, R. G.; Temkin, R. J. Microwave Field Distribution in a Magic Angle Spinning Dynamic Nuclear Polarization NMR Probe. *J. Magn. Reson.* **2011**, *210* (1), 16–23.
- (16) Lane, L. B. Freezing Points of Glycerol and Its Aqueous Solutions. *Ind. Eng. Chem.* **1925**, *17* (9), 924–924.
- (17) Barnes, A. B.; Markhasin, E.; Daviso, E.; Michaelis, V. K.; Nanni, E. A.; Jawla, S. K.; Mena, E. L.; DeRocher, R.; Thakkar, A.; Woskov, P. P.; Herzfeld, J.; Temkin, R. J.; Griffin, R. G. Dynamic Nuclear Polarization at 700 MHz/460 GHz. *J. Magn. Reson.* **2012**, *224*, 1–7.
- (18) Albert, B. J.; Pahng, S. H.; Alaniva, N.; Sesti, E. L.; Rand, P. W.; Saliba, E. P.; Scott, F. J.; Choi, E. J.; Barnes, A. B. Instrumentation for Cryogenic Magic Angle Spinning Dynamic Nuclear Polarization Using 90 L of Liquid Nitrogen per Day. *J. Magn. Reson.* **2017**, *283*, 71–78.
- (19) Matsuki, Y.; Fujiwara, T. Cryogenic Platforms and Optimized DNP Sensitivity. *eMagRes* **2018**, *7*, 9–24.
- (20) Bouleau, E.; Saint-Bonnet, P.; Mentink-Vigier, F.; Takahashi, H.; Jacquot, J.-F.; Bardet, M.; Aussenac, F.; Pureau, A.; Engelke, F.; Hediger, S.; Lee, D.; De Paëpe, G. Pushing NMR Sensitivity Limits Using Dynamic Nuclear Polarization with Closed-Loop Cryogenic Helium Sample Spinning. *Chem. Sci.* **2015**, *6* (12), 6806–6812.
- (21) Akbey, Ü.; Linden, A. H.; Oschkinat, H. High-Temperature Dynamic Nuclear Polarization Enhanced Magic-Angle-Spinning NMR. *Appl. Magn. Reson.* **2012**, *43* (1–2), 81–90.
- (22) Ni, Q. Z.; Markhasin, E.; Can, T. V.; Corzilius, B.; Tan, K. O.; Barnes, A. B.; Daviso, E.; Su, Y.; Herzfeld, J.; Griffin, R. G. Peptide and Protein Dynamics and Low-Temperature/DNP Magic Angle Spinning NMR. *J. Phys. Chem. B* **2017**, *121* (19), 4997–5006.
- (23) Concistrè, M.; Carignani, E.; Borsacchi, S.; Johannessen, O. G.; Mennucci, B.; Yang, Y.; Geppi, M.; Levitt, M. H. Freezing of Molecular Motions Probed by Cryogenic Magic Angle Spinning NMR. *J. Phys. Chem. Lett.* **2014**, *5* (3), 512–516.
- (24) Yi, X.; Fritzsching, K. J.; Rogawski, R.; Xu, Y.; McDermott, A. E. Contribution of Protein Conformational Heterogeneity to NMR Lineshapes at Cryogenic Temperatures. *Proc. Natl. Acad. Sci. U. S. A.* **2024**, *121* (8), No. e2301053120.
- (25) Akbey, Ü.; Franks, W. T.; Linden, A.; Lange, S.; Griffin, R. G.; van Rossum, B.-J.; Oschkinat, H. Dynamic Nuclear Polarization of Deuterated Proteins. *Angew. Chem., Int. Ed.* **2010**, *49* (42), 7803–7806.
- (26) Linden, A. H.; Franks, W. T.; Akbey, Ü.; Lange, S.; Van Rossum, B.-J.; Oschkinat, H. Cryogenic Temperature Effects and Resolution upon Slow Cooling of Protein Preparations in Solid State NMR. *J. Biomol. NMR* **2011**, *51* (3), 283–292.
- (27) Siemer, A. B.; Huang, K.-Y.; McDermott, A. E. Protein Linewidth and Solvent Dynamics in Frozen Solution NMR. *PLoS One* **2012**, *7* (10), No. e47242.
- (28) Du, J. L.; Eaton, G. R.; Eaton, S. S. Temperature, Orientation, and Solvent Dependence of Electron Spin-Lattice Relaxation Rates for Nitroxyl Radicals in Glassy Solvents and Doped Solids. *J. Magn. Reson. A* **1995**, *115* (2), 213–221.
- (29) Kuzhelev, A. A.; Strizhakov, R. K.; Krumkacheva, O. A.; Polienko, Y. F.; Morozov, D. A.; Shevelev, G. Yu.; Pyshnyi, D. V.; Kirilyuk, I. A.; Fedin, M. V.; Bagryanskaya, E. G. Room-Temperature Electron Spin Relaxation of Nitroxides Immobilized in Trehalose: Effect of Substituents Adjacent to NO-Group. *J. Magn. Reson.* **2016**, *266*, 1–7.
- (30) Sato, H.; Kathirvelu, V.; Fielding, A.; Blinco, J. P.; Micallef, A. S.; Bottle, S. E.; Eaton, S. S.; Eaton, G. R. Impact of Molecular Size on Electron Spin Relaxation Rates of Nitroxyl Radicals in Glassy Solvents between 100 and 300 K. *Mol. Phys.* **2007**, *105* (15–16), 2137–2151.
- (31) Sato, H.; Bottle, S. E.; Blinco, J. P.; Micallef, A. S.; Eaton, G. R.; Eaton, S. S. Electron Spin-Lattice Relaxation of Nitroxyl Radicals in Temperature Ranges That Span Glassy Solutions to Low-Viscosity Liquids. *J. Magn. Reson.* **2008**, *191* (1), 66–77.
- (32) Lelli, M.; Chaudhari, S. R.; Gajan, D.; Casano, G.; Rossini, A. J.; Ouari, O.; Tordo, P.; Lesage, A.; Emsley, L. Solid-State Dynamic Nuclear Polarization at 9.4 and 18.8 T from 100 K to Room Temperature. *J. Am. Chem. Soc.* **2015**, *137* (46), 14558–14561.
- (33) Menzildjian, G.; Lund, A.; Yulikov, M.; Gajan, D.; Niccoli, L.; Karthikeyan, G.; Casano, G.; Jeschke, G.; Ouari, O.; Lelli, M.; Lesage, A. Efficient Dynamic Nuclear Polarization up to 230 K with Hybrid BDPA-Nitroxide Radicals at a High Magnetic Field. *J. Phys. Chem. B* **2021**, *125* (48), 13329–13338.
- (34) Kaushik, M.; Lingua, H.; Stevanato, G.; Elokova, M.; Lelli, M.; Lesage, A.; Ouari, O. Trehalose Matrices for High Temperature Dynamic Nuclear Polarization Enhanced Solid State NMR. *Phys. Chem. Chem. Phys.* **2022**, *24* (20), 12167–12175.
- (35) Lee, D.; Chaudhari, S. R.; De Paëpe, G. Solvent Signal Suppression for High-Resolution MAS-DNP. *J. Magn. Reson.* **2017**, *278*, 60–66.
- (36) Yarava, J. R.; Chaudhari, S. R.; Rossini, A. J.; Lesage, A.; Emsley, L. Solvent Suppression in DNP Enhanced Solid State NMR. *J. Magn. Reson.* **2017**, *277*, 149–153.

- (37) Costello, W. N.; Xiao, Y.; Mentink-Vigier, F.; Kragelj, J.; Frederick, K. K. DNP-Assisted Solid-State NMR Enables Detection of Proteins at Nanomolar Concentrations in Fully Protonated Cellular Milieu. *J. Biomol. NMR* **2024**, *78*, 95.
- (38) Kang, X.; Zhao, W.; Dickwella Widanage, M. C.; Kirui, A.; Ozdenvar, U.; Wang, T. CCMRD: A Solid-State NMR Database for Complex Carbohydrates. *J. Biomol. NMR* **2020**, *74* (4–5), 239–245.
- (39) Biedenbänder, T.; Aladin, V.; Saeidpour, S.; Corzilius, B. Dynamic Nuclear Polarization for Sensitivity Enhancement in Biomolecular Solid-State NMR. *Chem. Rev.* **2022**, *122* (10), 9738–9794.
- (40) Ghassemi, N.; Poulhazan, A.; Deligey, F.; Mentink-Vigier, F.; Marcotte, I.; Wang, T. Solid-State NMR Investigations of Extracellular Matrixes and Cell Walls of Algae, Bacteria, Fungi, and Plants. *Chem. Rev.* **2022**, *122* (10), 10036–10086.
- (41) Duvvuri, K.; Richert, R. Binary Glass-Forming Materials: Mixtures of Sorbitol and Glycerol. *J. Phys. Chem. B* **2004**, *108* (29), 10451–10456.
- (42) Angell, C. A.; Sare, J. M.; Sare, E. J. Glass Transition Temperatures for Simple Molecular Liquids and Their Binary Solutions. *J. Phys. Chem.* **1978**, *82* (24), 2622–2629.
- (43) Mentink-Vigier, F.; Marin-Montesinos, I.; Jagtap, A. P.; Halbritter, T.; van Tol, J.; Hediger, S.; Lee, D.; Sigurdsson, S. Th.; De Paëpe, G. Computationally Assisted Design of Polarizing Agents for Dynamic Nuclear Polarization Enhanced NMR: The AsymPol Family. *J. Am. Chem. Soc.* **2018**, *140* (35), 11013–11019.
- (44) Harrabi, R.; Halbritter, T.; Alarab, S.; Chatterjee, S.; Wolska-Pietkiewicz, M.; Damodaran, K. K.; Van Tol, J.; Lee, D.; Paul, S.; Hediger, S.; Sigurdsson, S. Th.; Mentink-Vigier, F.; De Paëpe, G. AsymPol-TEKs as Efficient Polarizing Agents for MAS-DNP in Glass Matrices of Non-Aqueous Solvents. *Phys. Chem. Chem. Phys.* **2024**, *26* (6), 5669–5682.
- (45) Chatterjee, S.; Venkatesh, A.; Sigurdsson, S. Th.; Mentink-Vigier, F. Role of Protons in and around Strongly Coupled Nitroxide Biradicals for Cross-Effect Dynamic Nuclear Polarization. *J. Phys. Chem. Lett.* **2024**, *15* (8), 2160–2168.
- (46) Sibik, J.; Shalae, E. Y.; Axel Zeitler, J. Glassy Dynamics of Sorbitol Solutions at Terahertz Frequencies. *Phys. Chem. Chem. Phys.* **2013**, *15* (28), 11931.
- (47) Gordon, M.; Taylor, J. S. Ideal Copolymers and the Second-Order Transitions of Synthetic Rubbers. i. Non-Crystalline Copolymers. *J. Appl. Chem.* **1952**, *2* (9), 493–500.
- (48) Skrdla, P. J.; Floyd, P. D.; Dell'Orco, P. C. The Amorphous State: First-Principles Derivation of the Gordon-Taylor Equation for Direct Prediction of the Glass Transition Temperature of Mixtures; Estimation of the Crossover Temperature of Fragile Glass Formers; Physical Basis of the “Rule of 2/3”. *Phys. Chem. Chem. Phys.* **2017**, *19* (31), 20523–20532.
- (49) Simha, R.; Boyer, R. F. On a General Relation Involving the Glass Temperature and Coefficients of Expansion of Polymers. *J. Chem. Phys.* **1962**, *37* (5), 1003–1007.
- (50) Zograf, G.; Newman, A. Interrelationships Between Structure and the Properties of Amorphous Solids of Pharmaceutical Interest. *J. Pharm. Sci.* **2017**, *106* (1), 5–27.
- (51) Koop, T.; Bookhold, J.; Shiraiwa, M.; Pöschl, U. Glass Transition and Phase State of Organic Compounds: Dependency on Molecular Properties and Implications for Secondary Organic Aerosols in the Atmosphere. *Phys. Chem. Chem. Phys.* **2011**, *13* (43), 19238–19255.
- (52) Drake, A. C.; Lee, Y.; Burgess, E. M.; Karlsson, J. O. M.; Eroglu, A.; Higgins, A. Z. Effect of Water Content on the Glass Transition Temperature of Mixtures of Sugars, Polymers, and Penetrating Cryoprotectants in Physiological Buffer. *PLoS One* **2018**, *13* (1), No. e0190713.
- (53) Li, D.-X.; Liu, B.-L.; Liu, Y.; Chen, C. Predict the Glass Transition Temperature of Glycerol-Water Binary Cryoprotectant by Molecular Dynamic Simulation. *Cryobiology* **2008**, *56* (2), 114–119.
- (54) Talja, R. A.; Roos, Y. H. Phase and State Transition Effects on Dielectric, Mechanical, and Thermal Properties of Polyols. *Thermochim. Acta* **2001**, *380* (2), 109–121.
- (55) Prisco, N. A.; Pinon, A. C.; Emsley, L.; Chmelka, B. F. Scaling Analyses for Hyperpolarization Transfer across a Spin-Diffusion Barrier and into Bulk Solid Media. *Phys. Chem. Chem. Phys.* **2021**, *23* (2), 1006–1020.
- (56) Harrabi, R.; Halbritter, T.; Aussenac, F.; Dakhlaoui, O.; van Tol, J.; Damodaran, K. K.; Lee, D.; Paul, S.; Hediger, S.; Mentink-Vigier, F.; Sigurdsson, S. Th.; De Paëpe, G. Highly Efficient Polarizing Agents for MAS-DNP of Proton-Dense Molecular Solids. *Angew. Chem., Int. Ed.* **2022**, *61* (12), No. e202114103.
- (57) Becker-Baldus, J.; Yeliseev, A.; Joseph, T. T.; Sigurdsson, S. Th.; Zoubak, L.; Hines, K.; Iyer, M. R.; van den Berg, A.; Stepnowski, S.; Zmuda, J.; Gawrisch, K.; Glaubitz, C. Probing the Conformational Space of the Cannabinoid Receptor 2 and a Systematic Investigation of DNP-Enhanced MAS NMR Spectroscopy of Proteins in Detergent Micelles. *ACS Omega* **2023**, *8* (36), 32963–32976.
- (58) Mentink-Vigier, F.; Vega, S.; De Paëpe, G. Fast and Accurate MAS-DNP Simulations of Large Spin Ensembles. *Phys. Chem. Chem. Phys.* **2017**, *19* (5), 3506–3522.
- (59) Li, G.; Dastrup, B.; Palani, R. S.; Shapiro, M. A.; Jawla, S. K.; Griffin, R. G.; Nelson, K. A.; Temkin, R. J. Design and Optimization of THz Coupling in Zirconia MAS Rotors for Dynamic Nuclear Polarization NMR. *J. Magn. Reson.* **2024**, *364*, 107722.
- (60) Scott, F. J.; Dubroca, T.; Schurko, R. W.; Hill, S.; Long, J. R.; Mentink-Vigier, F. Characterization of Dielectric Properties and Their Impact on MAS-DNP NMR Applications. *J. Magn. Reson.* **2024**, *365*, 107742.
- (61) Kubicki, D. J.; Rossini, A. J.; Pura, A.; Zagdoun, A.; Ouari, O.; Tordo, P.; Engelke, F.; Lesage, A.; Emsley, L. Amplifying Dynamic Nuclear Polarization of Frozen Solutions by Incorporating Dielectric Particles. *J. Am. Chem. Soc.* **2014**, *136* (44), 15711–15718.
- (62) Geiger, M.-A.; Orwick-Rydmark, M.; Märker, K.; Franks, W. T.; Akhmetzhanov, D.; Stöppler, D.; Zinke, M.; Specker, E.; Nazaré, M.; Diehl, A.; van Rossum, B.-J.; Aussenac, F.; Prisner, T.; Akbey, Ü.; Oschkinat, H. Temperature Dependence of Cross-Effect Dynamic Nuclear Polarization in Rotating Solids: Advantages of Elevated Temperatures. *Phys. Chem. Chem. Phys.* **2016**, *18* (44), 30696–30704.
- (63) Mentink-Vigier, F.; Akbey, Ü.; Oschkinat, H.; Vega, S.; Feintuch, A. Theoretical Aspects of Magic Angle Spinning - Dynamic Nuclear Polarization. *J. Magn. Reson.* **2015**, *258*, 102–120.
- (64) Mentink-Vigier, F.; Paul, S.; Lee, D.; Feintuch, A.; Hediger, S.; Vega, S.; De Paëpe, G. Nuclear Depolarization and Absolute Sensitivity in Magic-Angle Spinning Cross Effect Dynamic Nuclear Polarization. *Phys. Chem. Chem. Phys.* **2015**, *17* (34), 21824–21836.
- (65) Thurber, K. R.; Tycko, R. Theory for Cross Effect Dynamic Nuclear Polarization under Magic-Angle Spinning in Solid State Nuclear Magnetic Resonance: The Importance of Level Crossings. *J. Chem. Phys.* **2012**, *137* (8), 084508.
- (66) Kundu, K.; Mentink-Vigier, F.; Feintuch, A.; Vega, S. DNP Mechanisms. *eMagRes* **2019**, *8*, 295–338.
- (67) Ghosh, M.; Sadhukhan, S.; Dey, K. K. Elucidating the Internal Structure and Dynamics of  $\alpha$ -Chitin by 2DPASS-MAS-NMR and Spin-Lattice Relaxation Measurements. *Solid State Nucl. Magn. Reson.* **2019**, *97*, 7–16.
- (68) Bougault, C.; Ayala, I.; Vollmer, W.; Simorre, J.-P.; Schanda, P. Studying Intact Bacterial Peptidoglycan by Proton-Detected NMR Spectroscopy at 100 kHz MAS Frequency. *J. Struct. Biol.* **2019**, *206* (1), 66–72.
- (69) Fernando, L. D.; Dickwella Widanage, M. C.; Penfield, J.; Lipton, A. S.; Washton, N.; Latgé, J.-P.; Wang, P.; Zhang, L.; Wang, T. Structural Polymorphism of Chitin and Chitosan in Fungal Cell Walls From Solid-State NMR and Principal Component Analysis. *Front. Mol. Biosci.* **2021**, *8*, 727053.
- (70) Rossini, A. J.; Widdifield, C. M.; Zagdoun, A.; Lelli, M.; Schwarzwälder, M.; Copéret, C.; Lesage, A.; Emsley, L. Dynamic Nuclear Polarization Enhanced NMR Spectroscopy for Pharmaceutical Formulations. *J. Am. Chem. Soc.* **2014**, *136* (6), 2324–2334.

(71) Pinon, A. C.; Schlagnitweit, J.; Berruyer, P.; Rossini, A. J.; Lelli, M.; Socie, E.; Tang, M.; Pham, T.; Lesage, A.; Schantz, S.; Emsley, L. Measuring Nano- to Microstructures from Relayed Dynamic Nuclear Polarization NMR. *J. Phys. Chem. C* **2017**, *121* (29), 15993–16005.

(72) Mathies, G.; Caporini, M. A.; Michaelis, V. K.; Liu, Y.; Hu, K.-N.; Mance, D.; Zweier, J. L.; Rosay, M.; Baldus, M.; Griffin, R. G. Efficient Dynamic Nuclear Polarization at 800 MHz/527 GHz with Trityl-Nitroxide Biradicals. *Angew. Chem.* **2015**, *127* (40), 11936–11940.

(73) Zhai, W.; Lucini Paioni, A.; Cai, X.; Narasimhan, S.; Medeiros-Silva, J.; Zhang, W.; Rockenbauer, A.; Weingarth, M.; Song, Y.; Baldus, M.; Liu, Y. Postmodification via Thiol-Click Chemistry Yields Hydrophilic Trityl-Nitroxide Biradicals for Biomolecular High-Field Dynamic Nuclear Polarization. *J. Phys. Chem. B* **2020**, *124* (41), 9047–9060.

(74) Wisser, D.; Karthikeyan, G.; Lund, A.; Casano, G.; Karoui, H.; Yulikov, M.; Menzildjian, G.; Pinon, A. C.; Pura, A.; Engelke, F.; Chaudhari, S. R.; Kubicki, D.; Rossini, A. J.; Moroz, I. B.; Gajan, D.; Copéret, C.; Jeschke, G.; Lelli, M.; Emsley, L.; Lesage, A.; Ouari, O. BDPA-Nitroxide Biradicals Tailored for Efficient Dynamic Nuclear Polarization Enhanced Solid-State NMR at Magnetic Fields up to 21.1 T. *J. Am. Chem. Soc.* **2018**, *140* (41), 13340–13349.

(75) Mentink-Vigier, F.; Mathies, G.; Liu, Y.; Barra, A.-L.; Caporini, M. A.; Lee, D.; Hediger, S.; G. Griffin, R.; De Paëpe, G. Efficient Cross-Effect Dynamic Nuclear Polarization without Depolarization in High-Resolution MAS NMR. *Chem. Sci.* **2017**, *8* (12), 8150–8163.

(76) Halbritter, T.; Harrabi, R.; Paul, S.; Van Tol, J.; Lee, D.; Hediger, S.; Sigurdsson, S. Th.; Mentink-Vigier, F.; De Paëpe, G. PyrroTriPol: A Semi-Rigid Trityl-Nitroxide for High Field Dynamic Nuclear Polarization. *Chem. Sci.* **2023**, *14* (14), 3852–3864.

(77) Yao, R.; Beriashvili, D.; Zhang, W.; Li, S.; Safeer, A.; Gurinov, A.; Rockenbauer, A.; Yang, Y.; Song, Y.; Baldus, M.; Liu, Y. Highly Bioresistant, Hydrophilic and Rigidly Linked Trityl-Nitroxide Biradicals for Cellular High-Field Dynamic Nuclear Polarization. *Chem. Sci.* **2022**, *13* (47), 14157–14164.

(78) Pura, A.; Reiter, C.; Dimitriadis, A. I.; de Rijk, E.; Aussenac, F.; Sergeyev, I.; Rosay, M.; Engelke, F. Improved Waveguide Coupling for 1.3 Mm MAS DNP Probes at 263 GHz. *J. Magn. Reson.* **2019**, *302*, 43–49.

(79) Aladin, V.; Corzilius, B. Methyl Dynamics in Amino Acids Modulate Heteronuclear Cross Relaxation in the Solid State under MAS DNP. *Solid State Nucl. Magn. Reson.* **2019**, *99*, 27–35.

(80) Aladin, V.; Vogel, M.; Binder, R.; Burghardt, I.; Suess, B.; Corzilius, B. Complex Formation of the Tetracycline-Binding Aptamer Investigated by Specific Cross-Relaxation under DNP. *Angew. Chem., Int. Ed.* **2019**, *58* (15), 4863–4868.

(81) Aladin, V.; Sreemantula, A. K.; Biedenbänder, T.; Marchanka, A.; Corzilius, B. Specific Signal Enhancement on an RNA-Protein Interface by Dynamic Nuclear Polarization. *Chem. - Eur. J.* **2023**, *29* (16), No. e202203443.

(82) Chaudhari, S. R.; Berruyer, P.; Gajan, D.; Reiter, C.; Engelke, F.; Silverio, D. L.; Copéret, C.; Lelli, M.; Lesage, A.; Emsley, L. Dynamic Nuclear Polarization at 40 kHz Magic Angle Spinning. *Phys. Chem. Chem. Phys.* **2016**, *18* (15), 10616–10622.

(83) Berruyer, P.; Björgvinsdóttir, S.; Bertarello, A.; Stevanato, G.; Rao, Y.; Karthikeyan, G.; Casano, G.; Ouari, O.; Lelli, M.; Reiter, C.; Engelke, F.; Emsley, L. Dynamic Nuclear Polarization Enhancement of 200 at 21.15 T Enabled by 65 kHz Magic Angle Spinning. *J. Phys. Chem. Lett.* **2020**, *11* (19), 8386–8391.